Journal of Cardiology 74 (2019) 182–188

Contents lists available at ScienceDirect

Journal of Cardiology

journal homepage: www.elsevier.com/locate/jjcc

Original article

3D printing and biocompatibility study of a new biodegradable occluder for cardiac defect

Yiming Sun (MD)[a,1], Xingjian Zhang (MD)[b,1], Wenjing Li (MD)[c], Yong Di (MD)[d], Quansheng Xing (MD, PhD)[d,*], Qian Cao (MD)[d]

[a] Medical College, Qingdao University, Qingdao, China
[b] Department of Cardiovascular Surgery, Jinan No. 4 Hospital, 1946 Jinan Shandong, Jinan, China
[c] Department of Gynecology, The Affiliated Hospital of Qingdao University, Qingdao, China
[d] Department of Cardiac Center, The Affiliated Women and Children's Hospital of Qingdao University, Qingdao, China

ARTICLE INFO

Article history:
Received 31 October 2018
Received in revised form 31 December 2018
Accepted 2 February 2019
Available online 23 March 2019

Keywords:
Congenital heart disease
Biocompatibility
3D printing
Occluder

ABSTRACT

Objective: To fabricate a biodegradable occluder for heart defect using the three-dimensional (3D) printing technique and evaluate its biosafety in an animal model.
Methods: Occluder samples were made by 3D printing technique using the self-developed lactide-sanya methyl carbonate-glycolide (PLLA-TMC-GA) co-polymer or PLTG as the bio-material. The biocompatibility (cytological and hematological) of the materials was evaluated by cytotoxicity experiments, hemolysis test, dynamic blood clotting test, and platelet adhesion test. Finally, the histocompatibility of the occluder was evaluated by implantation in a rabbit model.
Results: Occluder samples were printed satisfactorily. Cytotoxicity assay showed no significant toxicity of PLTG in the cells. Hemolysis test showed less than 5% hemolysis rate of PLTG indicating only a mild effect on the red blood cells. The dynamic coagulation test showed poor activation of endogenous clotting factors. PLTG resulted in lower platelet activation compared to PLLA, as indicated by the platelet adhesion test. Finally, no obvious tissue damage or necrosis was seen in the in vivo implantation experiment.
Conclusion: A new PLTG-based biodegradable occluder for heart defects with good biocompatibility can be manufactured by the 3D printing technique.

Introduction

Congenital heart disease is the most common birth defect in China, accounting for approximately 46.7% of all cases [1]. Transcatheter closure of septal defects with occluder devices shows a good short-term outcome. However, long-term clinical follow-up showed that the nickel-titanium alloy of the devices results in complications such as nickel ion hypersensitivity or toxicity [2–5]. Various groups [1,6–8] have explored the use of biodegradable materials such as polydioxanone (PDO) and poly L lactic acid (PLLA) in fabricating occluders. However, compared to the traditional Amplatzer occluder, the experimental results did not reach the expected level. In this study, we used the PLLA-TMC-GA terpolymer (PLTG) [9], consisting of PLLA, trimethylene carbonate (TMC) and glycolide (GA), and the 3D printing technology creatively to produce personalized occluders. We then evaluated its biological safety in in vitro and in vivo models. Our results provide the proof for further application of 3D printed bio-occluders.

Materials and methods

Preparation of PLTG extract

Since the occluder sample material was insoluble in water, as per the ISO 10993-12:2012 standard, the following procedure was used to obtain a PLTG extract for in vitro experiments. A 10 mm × 30 mm piece of the material was cut according to the standard recommended (surface area)/(recovery media mass) of 6 cm^2/ml and transferred to a closed sterile container. The piece

* Corresponding author at: Department of Cardiac Center, The Affiliated Women and Children's Hospital of Qingdao University, No. 6 Tongfu Road, Shibei District, Qingdao 266034, China.
E-mail address: xingqs0532@163.com (Q. Xing).
[1] These authors contributed equally to this work.

https://doi.org/10.1016/j.jjcc.2019.02.002
0914-5087/

was saturated in 50 ml physiological saline, and the container was placed in a constant-temperature drying oven. After drying for 72 h at (37 ± 1) °C, the container was cooled to room temperature, and vigorously shaken for 30 s to obtain the extract. The latter was transferred to another sterile container and sealed until use.

Design and preparation of occluder

The preliminary occluder design, vis-à-vis its unique shape and size, was calculated based on the location, size, and shape of the cardiac defect in various clinical cases, and the shape, size, and sheathing method of clinically used occluders.

The PLTG was dissolved in dichloromethane and then precipitated with ethanol to remove unreacted monomers and oligomers. After purification and drying, the copolymer was redissolved in methylene chloride. The solution was placed in an open flat-bottomed vessel, and the solvent was evaporated at room temperature for 48 h to obtain a dry printed material film. The film was crushed and dried under vacuum at 60 °C for 4 h to constant weight. The dried material was placed in the print cartridge, and the 3D model files of the STL format made by the CAD software were converted to the file types which were able to be recognized by the 3D printer. The bio-printer control software AnyPrint (Qingdao Unique Technology Co., Ltd., Qingdao, China) was used to retrieve the parameters of the upper and lower models of the occluder. Printing started after warming the print head to 150 °C. The printing parameters were set to: print speed – 4 mm/s, print temperature – 140 °C, layer thickness – 0.2 mm, discharge speed – 0.012 g/s, and nozzle diameter – 0.3 mm.

Cytotoxicity experiments

The effects of different concentrations (100%, 75%, 50%, 25%, 12.5%) of PLTG extract, sterile PBS (phosphate buffer saline, used as negative control), and 0.5% phenol solution (positive control) was tested on L929 cells. The cells were seeded into 96-well plate at the density of 5×10^4 ml^{-1} (100 μl per well) and incubated overnight. The PLTG extracts were then added, with a positive and a negative control well for each concentration of PLTG. After another 24 or 48 h incubation under 5% CO_2 at 37 (±1) °C, the cells were observed microscopically. To assess their viability, 10 μl of MTT (thiazolyl blue tetrazolium bromide) solution (5 mg/ml) was added to each well and the cells were incubated for an additional 4 h. The supernatants were removed and 150 μl DMSO (dimethyl sulphoxide) was added to each well. After shaking at low speed for 10 min, the absorbance (OD) of each well was measured at 490 nm. The cell viability was calculated using the following formula: cell viability (RGR) = $OD_{490a}/OD_{490b} \times 100\%$, where OD_{490a} is the absorbance of the test sample well and OD_{490b} is the absorbance of the blank wells.

Hemolysis test

New Zealand white rabbits were used for the blood compatibility experiments. To collect blood, the rabbits were anesthetized by ear vein injection of 3% pentobarbital sodium at 1 ml/kg. For all blood compatibility tests, blood was aspirated from the heart into a 10-ml syringe rinsed with 1 ml ACD (acid citrate dextrose) anticoagulant, and transferred into a 15-ml test tube pre-rinsed with anticoagulant.

Fresh rabbit blood was diluted with physiological saline (4:5) and 200 μl of the diluted sample was incubated with pre-warmed (30 min in a 37 °C water bath) PLTG extracts, distilled water (positive control), or normal saline (negative control) in a 37 °C water bath for 60 min. The tubes were centrifuged at 3000 rpm for 5 min and the supernatants were collected in separate tubes. The absorbance (A) of the supernatants were measured at 545 nm, and the hemolysis rate was calculated as follows: Hemolysis Rate (HR) = $(A_t - A_{nc})/(A_{pc} - A_{nc}) \times 100$, where A_t is the absorbance of PTGL, A_{nc} is the absorbance of the negative control, and A_{pc} is the absorbance of the positive control. A hemolytic rate greater than 5% indicated hemolytic effect. Each sample was tested in triplicates.

Dynamic coagulation test

Eighty microliters of fresh rabbit blood (blood:anticoagulant = 9:1) and 10 μl of 0.2 M $CaCl_2$ solution were added to 10 μl PLTG extract in a siliconized glass tube, 10 μl normal saline in a siliconized glass tube (negative control), or 10 μl normal saline in a non-silicified glass tube (positive control group), and mixed immediately. At different time points (0, 20, 40, 60, 80, 100, 120 min) post-mixing, 20 ml pure water was poured onto the blood surface, and 200 μl of the solution was transferred from each tube to a 96-well plate to measure the absorbance (OD) at 540 nm. Each sample at each time point was measured in triplicates. The dynamic coagulation time curves of the samples were obtained by plotting the OD values vs. time.

Platelet adhesiveness test

Fresh rabbit blood was centrifuged at 1400 rpm for 10 min, the top 3/4th of the supernatant was collected and centrifuged again for 15 min, and again the top 3/4th of the supernatant, i.e. the platelet-poor plasma (PPP) was discarded. The remaining bottom 1/4th of the supernatant, i.e. the platelet-rich plasma (PRP), was collected for the test. A 0.5 cm × 0.5 cm piece each of PLTG and the clinically approved PLLA (control material) was irradiated with ultraviolet light for 2 h, immersed in PBS buffer (pH = 7.4) for 4 h, and then incubated in PRP at 37 °C for 1 h in a 96-well plate. The pieces were removed and washed thrice with PBS buffer to remove non-adsorbed platelets, and then immersed in 25 g/l glutaraldehyde in PBS for 30 min to fix the surface platelets. Finally, the pieces were successively dehydrated at room temperature in an ethanol gradient with 20 min in each concentration, until they reached the critical point of CO_2, after which gold was sprayed onto them. The adhesion of platelets to the material surfaces was observed by scanning electron microscopy (SEM), and platelets were counted. Adherent platelets are classified into 5 types based on the degree of deformation [10]: type I – disk-shaped, undeformed, type II – pseudopodia beginning to protrude but no flattening against the material, type III – more extended pseudopodia with incipient aggregation and flattening but no cell matrix in between the pseudopodia, type IV – flattened with cytoplasm beginning to spread between the pseudopodia and forming a network structure with fibrin, type V – completely extended cell matrix, no apparent pseudopodia and completely flattened against the material. The morphological index was calculated as follows:

Morphological index = (type I platelet count × 1 + type II platelet count × 2 + type III platelet count × 3 + type IV platelet count × 4 + type V platelet count × 5)/adherent platelets total. The greater the morphological index, the greater the degree of platelet deformation.

Histocompatibility test

Thirty New Zealand white rabbits were randomized into 5 groups (n = 6; regardless of sex) and kept in the same environment for 1 week. PLTG occluder discs, nickel titanium alloy tablets, and PLLA slices of similar dimensions were soaked in the 70% ethanol for 24 h, and washed with sterile PBS twice. In

every group, 2 rabbits each were implanted with the PLTG disk, NiTi alloy sheet or PLLA slices. After anesthetizing with 3% pentobarbital sodium (1 ml/kg) through the ear vein, the rabbits were affixed on the operating table through the limbs using 4 strings. After cleaning the skin along the spine, 2 implantation spots were chosen, with the distance between them no less than 5 cm. After labeling the operational spot with paint, the surgical field was disinfected by povidone iodine, and then covered with aseptic hole-towels. The skin, subcutaneous tissue and deep fascia were first incised, and a small blunt forceps was used to separate the muscle. The PLTG disk/NiTi alloy sheet/PLLA slices were implanted intra-muscularly. The rabbits were sutured conventionally without bandaging and cefazolin sodium (800,000 U) was injected intramuscularly once a day for 3 days. The general health, and any toxic/fatal reactions were observed in the postoperative period. One experimental group of rabbits was killed at 1, 4, 8, 12, and 16 weeks by euthanasia after weighing. The incised skin of back and the implantation site were resected and fixed in 10% formaldehyde for 48 h. After rinsing in flowing water, the fixed tissues were dehydrated in an ethanol gradient (10 min each), embedded in paraffin, and 5-μm thick sections were cut. The tissue sections were stained with hematoxylin and eosin and observed under the light microscope to observe any inflammatory reaction, formation of fibrous capsule, and degradation of the occluder materials.

Results

Occluder design and manufacture

The CAD software was used to design a preliminary 3D model of occluder using parameters of the existing occluders as reference, along with clinical data available on occluder use. The 3D printed occluder was 2 mm long and 4–10 mm in diameter double-disk dumbbell with a central, cylindrical waist. The two discs are 2 mm wider than the waist diameter.

The PLLA-TMC-GA copolymer easily forms bubbles during purification and drying. Direct processing by a 3D printer also has a high probability of bubble formation, which can render the material defective for medical use. Therefore, to obtain a bubble-free and stable material, it was solubilized in dichloromethane and then evaporated.

The length of the print occluder model was 10 mm, and the wall thickness was 0.6 mm. The diameter of the disk surface on both sides was 10 mm, the thickness was 2 mm, and the diameter of the middle shaft was 6 mm. The sample occluder was consistent with the CAD software design model. The disk had a uniform texture, with one smooth and one slightly rough side. Considering the reduction in the molecular weight of the material during high-temperature printing, the occluder exhibited good elasticity and toughness at 37 °C.

Cytotoxicity of the PLTG material

L929cells were treated with different concentrations of the PLTG extracts for 24 h and 48 h. The cells appeared shuttle-shaped, but the overall morphology was intact. In contrast, the control cells were spherical, and mostly suspended with no obvious adherence.

According to ISO 10993-5: 2009 standards for the biological evaluation of medical devices (Part: Tests for in vitro cytotoxicity), a relative cell survival rate less than 70% indicates potential cytotoxicity. Furthermore, for a material to pass this test, the relative cell survival rate at the 50% concentration must be greater than or equal to that at the 100% concentration. The cell viability at 100% PLTG at the 24 h and 48 h time points were 84.9% and 90.1% respectively, indicating that the material has no obvious cytotoxicity and good cell compatibility (Table 1).

Table 1
The absorbance and relative growth rate (RGR) of different groups.

Groups	OD value		RGR (%)	
	24 h	48 h	24 h	48 h
100%	0.270 ± 0.018	0.292 ± 0.011	84.9	90.1
75%	0.319 ± 0.012	0.321 ± 0.005	100.3	99.1
50%	0.311 ± 0.005	0.318 ± 0.011	97.8	98.1
25%	0.298 ± 0.009	0.310 ± 0.009	93.7	95.6
12.5%	0.318 ± 0.013	0.323 ± 0.013	100.0	99.7
Negative group	0.318 ± 0.006	0.324 ± 0.006	100.0	100.0
Positive group	0.134 ± 0.012	0.129 ± 0.008	42.1	39.8

RGR: relative growth rate; OD: optical density.

Hemolysis test

According to the GB14233.2-2005 standards for medical equipment, a suitable material should have $A_{pc} = 0.8 \pm 0.3$, $A_{nc} \leq 0.03$, and HR < 5%. The A_{pc}, A_{nc}, and HR value for PLTG were 0.8 ± 0.3, ≤0.03, and 2.5% respectively, indicating the PLTG is not hemolytic (Table 2).

Dynamic coagulation test

When blood initially starts to coagulate, the absorbance drops to 0.1, and when it is completely coagulated, the absorbance drops further to 0.01 [11]. The dynamic coagulation time curve of the PLTG extract (Fig. 1) showed that the absorbance of PLTG decreased gradually with time, similar to that in the negative control, indicating that PLTG poorly activated coagulation factor. The absorbance curve of the corresponding positive controls group showed a steeper decrease indicating highly activated coagulation factors.

Platelet adhesiveness test

Platelet adhesion to PLTG and PLLA surfaces were observed under 3000× and 10,000× magnification. The platelets were evenly distributed, and some platelets had protruded from the pseudopodia and started to activate. The platelet morphology was

Table 2
The results of hemolysis test.

Groups	OD-1	OD-2	OD-3	Mean value of OD
Sample group (ODt)	0.031	0.046	0.035	0.037
Negative group (ODnc)	0.019	0.082	0.014	0.018
Positive group (ODpc)	0.799	0.762	0.774	0.778

ODt, optical density (test sample); ODnc, optical density (negative control); ODpc, optical density (positive control).

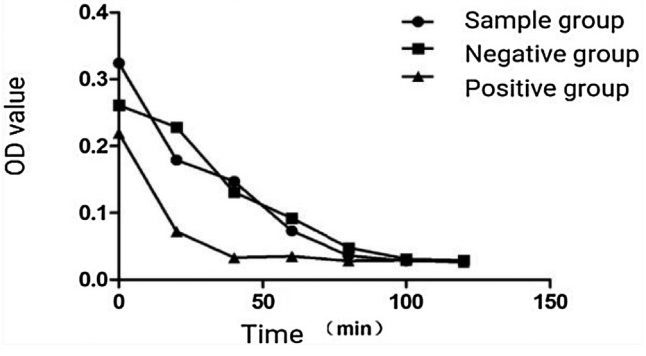

Fig. 1. The dynamic coagulation time curve of the PLTG extract.

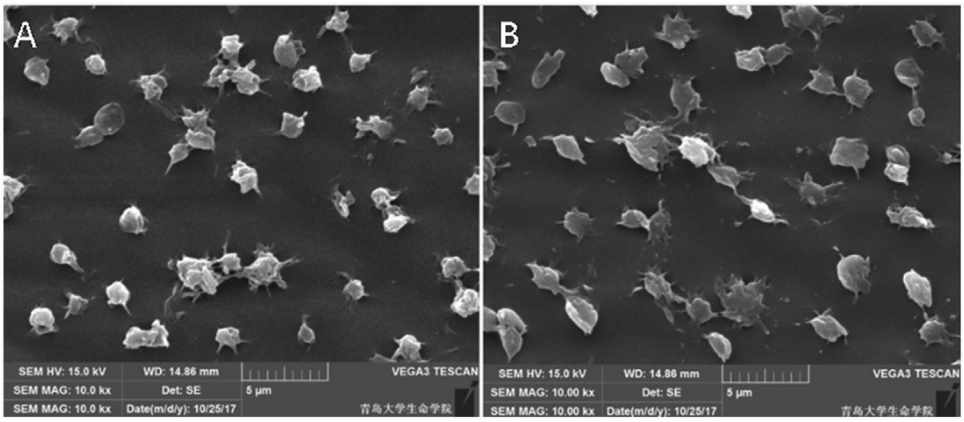

Fig. 2. Platelets adhering to different materials under the electron microscope (3000×, 10,000×).

observed using SEM in 6 different visual fields under 20,000 magnification (Fig. 2). Around 10–15 platelets were counted per field and classified according to their morphology. No significant differences were seen between the two groups; platelets adhering to both materials were deformed to varying degrees, and some platelets had extended pseudopodia. Comparison of the platelet morphology index (Table 3) showed that the degree of deformation of the platelets on PLTG was slightly better than that seen on PLLA.

Histocompatibility test

All 30 rabbits were implanted successfully with the respective materials and none of them died during the perioperative period. In addition, all animals displayed normal eating, defecation, and motion, and no infection or swelling was seen at the incision site. According to ISO 10993-12: 2012, ISO 10993-6:2007, and GB/T 16886.6-2015 criteria, the inflammatory scores consist of 2 parts: the first is the *Inflammatory cell infiltration pertaining to the soft tissue*, Class I – No or only a very few lymphocytes around the sample; Class II – A few lymphocytes around the sample; Class III– A small amount of neutrophils and lymphocytes infiltration as well as the giant cell reaction around the sample; Class IV– Inflammatory reaction mainly caused by infiltration of the neutrophils, and macrophages are visible. The second is the *Grading criteria for the formation of fibrous capsule walls*, Class 1 – The thickness of the cyst wall is stable, and no continuous proliferation occurs; Class 2 – Capsular space of fibrosis is compact, and the thickness of the wall is thinner than initial stage; Class 3 – Fibroblasts, fibrocytes, and collagenous fibers are visible in the surrounding tissue, with the fibrous cavity structure having already formed; Class 4 – Small vessels and fibroblasts proliferate around the sample, while the loose capsule wall begins to form. And 1 point, 2 points, 3 points, and 4 points were given for the Class IV (or 4), Class III (or 3), Class II (or 2), and Class I (or 1), respectively. Meanwhile, as per ISO/GB criteria mentioned above, the *Indicator of the national grades of histologic reaction* is listed as follows and is used to combine the points from the 2 parts mentioned above: at the time of 1 week, the inflammatory cells reaction should be ≤Class IV, while the formation of the fibrous cyst wall should present no fibrous cyst wall formation; at the time of 4 weeks, the inflammatory cells reaction should be ≤Class II, while the formation of the fibrous cyst wall should be ≤Class 4; at the time of 12 weeks, the inflammatory cells reaction should be ≤Class I, while the formation of the fibrous cyst wall should be ≤Class 2; at the time of 16 weeks, the inflammatory cells reaction should be ≤Class I and the formation of the fibrous cyst wall should be ≤Class 1. If the appearance under the microscope tended to be in the middle of 2 grades, the higher grade would be chosen for evaluation. All the results were analyzed by SPSS 24 (Statistical Product and Service Solutions, IBM Corporation, New York, the US). Table 4 displays the data of the experiment in the form of mean ± standard deviation.

Sample group

One week after implantation, macroscopic observation showed no edema and congestion around the incised area, and new tissue had begun to form which was not easily distinguishable from the boundary of the muscle tissue. Microscopically, the new tissue consisted mainly of fibroblasts and macrophages, along with neutrophils, lymphocytes, and nascent capillaries. Four weeks post-implantation, the operated site was covered with a white fibrous tissue, which formed a thick- and loose-walled sac. Neither edema nor hyperemia was seen in the surrounding tissue. The layer adjacent to the occluder was the 'foam cell layer' consisting of the degraded occluder material that was phagocytized by the macrophages, followed by a layer of fibroblasts and finally a fibro-cellular layer next to the muscle tissue. The three-layer structure was arranged loosely, with visible capillaries and a small number of lymphocytes. Eight weeks after implantation, the fibrous sac wall was slightly thinner but tougher, and could still be microscopically distinguished from the occluder. The fibro-cellular and fibroblast layers were thinner and denser, but the foam cell layer was thicker, and a few multinucleated cells and plasma cells were also visible. Twelve weeks post-implantation, the fibrous sac wall was even thinner and tougher, and could easily be separated from the occluder samples. All three layers of sac wall were

Table 3
The amount of platelets adhering to different materials and the morphology index.

Groups	The amount of adhered platelets					Total	Morphology index
	Type I	Type II	Type III	Type IV	Type V		
Sample group	15	22	24	12	3	76	2.55
PLLA group	12	20	30	17	3	82	2.74

PLLA, poly L lactic acid.

Table 4
Inter-subject effect test.

Item	Type III SS	df	Mean square	*F*	*P* value[b]
Correction model	241.900[a]	14	17.279	35.749	0.000
Weeks	228.567	4	57.142	118.224	0.000
Material kinds	4.900	2	2.450	5.069	0.010
Weeks × Material kinds	8.433	8	1.054	2.181	0.047
Discrepancy	21.750	45	0.483		
Total	1561.000	60			
Corrected total	263.650	59			

As it is shown in Table 4, the *P* value of the Weeks × Material kinds does exist (with *P* value = 0.047 < 0.05), so the post hoc test needs to be done to find which one has better histocapatibility with surrounding tissue.
[a] *R*-square = 0.918 (adjusted *R*-square = 0.892).
[b] The significant level is 0.05.

thinner, and the boundary between the fibro-cellular and fibroblast layers was blurred. Sixteen weeks after the implantation, no obvious change was seen in the fibrous sac structure. The wall thickness was stable, but the boundaries between the individual layers were not very clear, and the foam cells were visible between the fibro-cellular and fibroblast layers. In addition, a few lymphocytes could also be found occasionally (Fig. 3A–C).

Nickel-titanium alloy group

Gradual changes were also seen in connective tissue post implantation. One week after operation, proliferative connective tissue formed loose and slightly thick capsule wall, and a large number of round cells and fibroblasts formed the cyst wall. Four weeks after the operation, the capsule wall thinned as collagen fibers started to form, and incipient neovascularization could be seen around the site. Eight weeks after the operation, the proliferative reaction of connective tissue in some specimens was still obvious with a thick wall and presence of some giant cells. Another four weeks later, the cyst wall became thinner and more stable. After sixteen weeks since the operation, there was no proliferation in the cyst wall, and only a small number of lymphocytes could be seen around the site (Fig. 3G–I).

PLLA film group

After 1 week of the implantation, edema in the surrounding tissue was visible macroscopically. Neutrophils, fibroblasts, and macrophages accounted for the major parts of the inflammatory reaction under the microscope, and the wall of the sac was loose. Four weeks after the implantation, the PLLA films were wrapped by the fibrous connective tissue, and the wall of the capsule became thicker with a tough texture. Neovascular and scattered lymphocytes could be found in the surrounding tissue of the implantation. Another four weeks later, a large amount of inflammatory cells was seen around the implantation spot, with an integral shape of the sample and obvious hyperplasia of the surrounding tissue. Twelve weeks after the operation, the extent of the inflammatory reaction decreased and the materials began to degrade, but the macroscopic shape still existed with a layer of flat cells (it was soon proved as endothelial cells by CD34 immunohistochemical staining) on the surface of the material. And the neovascularization appeared near the PLLA films. At 16 weeks, there was no inflammation, some degraded parts of the materials were replaced by the fibrous connective tissue, and integral neovascularization was seen (Fig. 3D–F).

Data description

Analysis of variance was performed to determine any correlation between the time and the occluder material, which affected the inflammatory evaluation (Table 4). Since a slight correlation was observed ($p = 0.047$), a post hoc test was conducted to determine which material had better histocompatibility (Table 5). No significant differences were seen between PLTG and nickel-titanium alloy ($p = 0.118$), but PLTG was significantly different from PLLA ($p = 0.003$) in terms of histocompatibility.

Discussion

3D printing technology originated in the late 1980s and is highly promising in the medical field. With the help of clinical tomography (CT) data and a designing software (CAD), the printing materials can be accurately stacked layer by layer in the 3D plane for high throughput digital molding and manufacturing. It is a

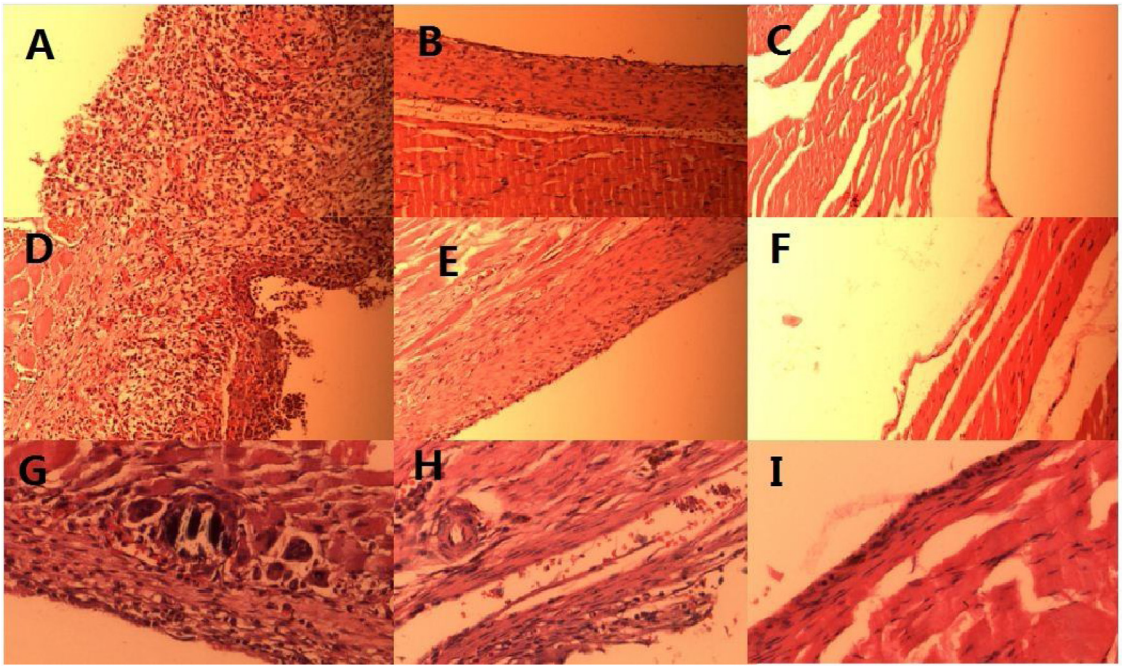

Fig. 3. (A–C) Samples 1 week, 4 weeks, and 12 weeks after the implantation, respectively; (D–F) poly L lactic acid 1 week, 4 weeks, and 12 weeks after the implantation, respectively; (G–I) Nitinol 1 week, 4 weeks, and 12 weeks after the implantation, respectively.

Table 5
Comparisons of inflammatory scores among different material groups.[b]

Material kind	Material kind	Mean difference	Standard error	*P* value [a]	95% Confidence interval	
					Lower limit	Upper limit
Ni-Ti alloy	PLLA	0.3500	0.21985	0.118	−0.0928	0.7928
	Test sample	−0.3500	0.21985	0.118	−0.7928	0.0928
PLLA	Ni-Ti alloy	−0.3500	0.21985	0.118	−0.7928	0.0928
	Test sample	−0.7000	0.21985	0.003	−1.1428	−0.2572
Test sample	Ni-Ti alloy	0.3500	0.21985	0.118	−0.0928	0.7928
	PLLA	0.7000	0.21985	0.003	0.2572	1.1428

What Table 5 illustrates is that compared with Nickel-titanium alloy, our material does not have significant difference (with the P value = 0.118 > 0.05), however, there is a statistically significant difference between our material and the PLLA (with the P value = 0.003 < 0.05).
[a] The significant level is 0.05.
[b] Multiple comparisons after factorial design.

rapid and integrated process that can be tailored to individual specifications. At present, this technology is mostly used in 3D jet printing (3DP), photo-curing (SLA), selective laser sintering (SLS), and fused deposition modeling (FDM). However, several researchers such as Guarino [12] and Yang [13] are actively exploring the application of this technology in medical and clinical fields. The 3D printing approach is particularly attractive in designing occluders used in the treatment of congenital heart diseases. Currently, they are manufactured in batches according to calibrated molds, which makes it difficult to perfectly match them to the shape and size of a patient's heart defect. Using clinical data as reference, 3D printing technology can help produce occluders according to patient specifications. We demonstrate the feasibility of the 3D printing technology in manufacturing septal defect occluders using a preliminary design created by the CAD software.

The bio-compatibility of a medical implantation is vital for it to be effectively repaired or reconstructed in the body [14]. Due to their good degradability and absorbability, PLLA, trimethylene (TMC) and glycolide (GA) have been used in some clinical applications. PLLA is also an ideal biomaterial [15] that has load-bearing function due to its good tensile strength [16] and modulus. It is widely used in tissue engineering stents, and has been approved by the US Food and Drug Administration for sutures and implants [17]. Although it has good histocompatibility and is degraded into lactic acid in vivo which can eventually be excreted via the tricarboxylic acid cycle [18–20], the continuous accumulation of lactic causes a sharp drop in the pH in the surrounding tissue and can trigger an inflammatory reaction [21]. Poly-TMC (PTMC) combines good mechanical properties and biodegradability with biocompatibility. Since its degradation products are neutral 1,3-propanediol and carbon dioxide, no acidity and inflammation ensue from using PTMC. It is currently used in fabricating controlled release materials. Poly-GA (PGA) is a non-toxic macromolecule which is ultimately degraded into water and carbon dioxide in vivo [22]. The greatest advantage of PGA is its mechanical strength which can be increased with increasing molecular weight, which makes it highly suitable for surgical sutures, as well as the fixation and repair of tendon injuries, fractures, and other tissue injuries. We have combined these three bio-materials into the PLLA-TMC-GA copolymer (PLTG) to design an occluder that combines the best properties of the individual components.

Whenever a foreign material is implanted in a tissue, the cells react to the stimulus with an inflammatory response, or even a complete rejection. In addition, if the implant is in direct contact with the blood, there is a considerable risk of activating the complement system which can cause hemolysis and thrombosis. Therefore, the most important requirement for an implant is its safety and biocompatibility. The latter encompasses cell, blood, and histocompatibility. Cell compatibility is measured in terms of the effect of the material on the composition, structure, and function of the cells with which it is in direct contact after implantation. According to ISO 10993-5:2009 standards, a relative cell survival rate less than 70% indicates potential cytotoxicity, thus, the cytotoxicity tests showed overall good cell-compatibility of PLTG. Good blood compatibility is measured in terms of lack of thrombosis and platelet activation, minimal platelet attachment, shortened clotting time, and inactivation of the coagulation system, no hemolysis, and no adverse reactions to other blood cells/components (it was exactly defined as per GB14233.2-2005 standards for medical equipment, a suitable material should have $A_{pc} = 0.8 \pm 0.3$, $A_{nc} \leq 0.03$, and HR < 5%). The rate of hemolysis induced by the implant directly reflects the strength of the interaction between the material and the red blood cells; the higher the hemolysis rate, the greater is the red blood cell destruction, and the lower is the blood compatibility. The implant material can also activate the endogenous coagulation pathway which increases the degree of blood coagulation with time. Dynamic coagulation assays (the closer the dynamic coagulation curve of the test sample to the mesoposition of two control groups, the better blood compatibility of the test sample will be) can measure the degree of activation of endogenous clotting factors. PLTG showed no hemolysis, poor coagulation, and minimal platelet adhesion (the smaller the degree of platelet deformation, the smaller the morphological index, and the better blood compatibility will be) confirming its good blood compatibility which meets implant requirements.

When a biological material is implanted in an animal, it eventually degrades. The degradation rate of the material is affected by multiple factors, such as its structure, shape, molecular weight, aggregation state, and hydrolysis temperature [23]. A biomaterial can be degraded by either non-enzymatic hydrolysis [24] or enzymatic hydrolysis [23] of ester bonds. Since small water molecules can easily penetrate the interior of the polymer, hydrolysis occurs both on the surface and interior of the occluder. Enzymes on the other hand are larger and do not easily penetrate the interior of the material. Therefore, enzymatic hydrolysis takes place on the polymer surface. Bio-degradation initially decreases the molecular weight of the polymer without significantly affecting its quality. This process is accompanied by the release of acidic degradation products, triggering an inflammatory response within one week of implantation. Gradually, the quality of the implant is reduced as the fragments fall off until the material is completely degraded. The particles that are shed from the implant can trigger an inflammatory reaction [25]. In our study, a large number of macrophages engulfed the degraded particles to form foam cells four weeks after implantation. Over time however, the number of foam cells gradually reduced as did the inflammatory response. While a severe inflammatory response is a sign of histo-incompatibility, a moderate response can in fact assist the

implantation by completing endothelialization. Studies show that the implanted occluder can achieve endothelialization after 3 months [26], after which the occluder still exists but is largely ineffective due to postoperative complications. Therefore, the optimum biomaterial should avoid triggering an inflammatory response before complete endothelialization.

In terms of histological effects, no significant differences were seen between PLTG and the nickel-titanium alloy which is routinely used in clinics, indicating that this novel co-polymer was comparable to a clinically tested material. PLTG however has advantage of biodegradability, which avoids the persistent reactions to metal toxicity. Furthermore, a significant difference was seen between PLTG and PLLA, which is widely being tested for biodegradable occluders. Therefore, our novel co-polymer not only causes less inflammatory damage but is also more stable than the PLLA. An ideal occlusion device needs to have a certain degree of elasticity and toughness to maintain its shape during sheathing and implantation and to perform its function. As PLTG appears to be a potential choice for a new generation of biodegradable occluders, our next steps are to optimize the transmission of PLTG occluder, such as matching it to the guide wire and insertion, and its shape.

Conclusion

A new biodegradable heart defect occluder can be designed and implemented using 3D printing technology. The cytotoxicity, hemolysis, coagulation, and platelet adhesion tests indicated good cell and blood compatibility of the PLLA-TMC-GA copolymers. Implantation in a rabbit model showed good histocompatibility and no systemic toxicity. In summary, the PLTG biodegradable occluder is safe and reliable, with overall good biocompatibility.

Funding

This research was supported by The National Natural Science Foundation of China (NSFC) [Grant numbers 81570287 and 81770315]; and the Achievement Transformation Plan of Qingdao (Grant no. 16-6-29-nsh).

Conflicts of interest

The authors declare that there is no conflict of interest.

References

[1] Zhu YF, Huang XM, Cao J, Hu JQ, Bai Y, Jiang HB, et al. Animal experimental study of the fully biodegradable atrial septal defect (ASD) occluder. J Biomed Biotechnol 2012;2012:735989.
[2] Raghu A, Kawalsky D, Feldman M. Embolic stroke due to a left atrial thrombus two years after placement of an atrial septal defect closure device. Am J Cardiol 2006;98:1294–6.
[3] Delaney JW, Li JS, Rhodes JF. Major complications associated with transcatheter atrial septal occluder implantation: a review of the medical literature and the manufacturer and user facility device experience (MAUDE) database. Congenit Heart Dis 2007;2:256–64.
[4] Crawford GB, Brindis RG, Krucoff MW, Mansalis BP, Carroll JD. Percutaneous atrial septal occluder devices and cardiac erosion: a review of the literature. Catheter Cardiovasc Interv 2012;80:157–67.
[5] Happel CM, Laser KT, Sigler M, Kececioglu D, Sandica E, Haas NA. Single center experience: implantation failures, early, and late complications after implantation of a partially biodegradable ASD/PFO-device (BioStar®). Catheter Cardiovasc Interv 2015;85:990–7.
[6] Hoehn R, Hesse C, Ince H, Peuster M. First experience with the BioSTAR-device for various applications in pediatric patients with congenital heart disease. Catheter Cardiovasc Interv 2010;75:72–7.
[7] Dai K, Li F, Sun K, Dou HJ, Sun K, Wang YH, et al. Experimental ASD closure using a fully biodegradable ASD occluder in swine models. J Clin Pediatr 2010;28:375–9.
[8] Huang XM, Zhu YF, Cao J, Hu JQ, Bai Y, Jiang HB, et al. Development and preclinical evaluation of a biodegradable ventricular septal defect occluder. Catheter Cardiovasc Interv 2013;81:324–30.
[9] Dong J, Liao L, Shi L, Tan Z, Fan Z, Li S, et al. A bioresorbable cardiovascular stent prepared from L-lactide, trimethylene carbonate and glycolide terpolymers. Polym Eng Sci 2014;54:1418–26.
[10] Ko TM, Lin JC, Cooper SL. Surface characterization and platelet adhesion studies of plasma-sulphonated polyethylene. Biomaterials 1993;14:657–64.
[11] Ren L, Xu L, Feng J, Zhang Y, Yang K. In vitro study of role of trace amount of Cu release from Cu-bearing stainless steel targeting for reduction of in-stent restenosis. J Mater Sci Mater Med 2012;23:1235–45.
[12] Guarino J, Tennyson S, McCain G, Bond L, Shea K, King H. Rapid prototyping technology for surgeries of the pediatric spine and pelvis: benefits analysis. J Pediatr Orthop 2007;27:955–60.
[13] Yang J, Cai H, Lv J, Zhang K, Leng H, Sun C, et al. In vivo study of a self-stabilizing artificial vertebral body fabricated by electron beam melting. Spine (Phila Pa 1976) 2014;39:E486–92.
[14] Wu QY, Zhou WY, He MY, Chen Q. Synthesis of glycolide. Fine Chem 2012;29:413–6.
[15] Fan X, Chen J, Ruan JM, Zou JP, Zhou ZC, Liu Y, et al. Research and progress on polylactide biodegradable materials. Mater Sci Eng Powder Met 2008;4:187–94.
[16] Chandrasekaran S, Ramachandran A, Eapen A, George A. Stimulation of periodontal ligament stem cells by dentin matrix protein 1 activates mitogen-activated protein kinase and osteoblast differentiation. J Periodontol 2013;84:389–95.
[17] Shi SX. Studies on the preparation and degradation of polylactide and copolymers[D]. Beijing University of Chemical Technology; 2007. p. 1–129.
[18] Liu Q, Mo AC. Effect of yttrium/hydroxyapatite nanoparticles on the biological behavior of human periodontal ligament cells. Chinese J Conserv Dentistry 2008;3:139–43.
[19] Mao Z, Yin Y, Mao X, Chu CL. Morphology of elderly people's periodontal ligament cells attached to the three-dimensional porous nano-hydroxylapatite. J Med Postgrad 2009;22:815–8.
[20] Liu W, Konermann A, Guo T, Jäger A, Zhang L, Jin Y. Canonical Wnt signaling differently modulates osteogenic differentiation of mesenchymal stem cells derived from bone marrow and from periodontal ligament under inflammatory conditions. Biochim Biophys Acta 2014;1840:1125–34.
[21] Sanger C, Soto A, Mussa F, Sanzo M, Sardo L, Donati PA, et al. Maximizing results in craniofacial surgery with bioresorbable fixation devices. J Craniofac Surg 2007;18:926–30.
[22] Maurus PB, Kaeding CC. Bioabsorbable implant material review. Oper Tech Sports Med 2004;12:158–60.
[23] Kaplan DL. Introduction to biopolymers from renewable resources. Biopolymers from renewable resources. Berlin Heidelberg: Springer; 1998. p. 1–29.
[24] Pêgo AP, Van Luyn MJ, Brouwer LA, van Wachem PB, Poot AA, Grijpma DW, et al. In vivo behavior of poly (1,3-trimethylene carbonate) and copolymers of 1,3-trimethylene carbonate with D,L-lactide or epsilon-caprolactone: degradation and tissue response. J Biomed Mater Res A 2003;67:1044–54.
[25] Bai B, Ye MC. The current situation and future extracellular matrix materials in bone tissue engineering. Prog Modern Biomed 2007;7:138–41.
[26] Hu JQ, Qin YW, Wang SQ, Zhao XX, Zhou BY, Xiong WF. Evaluation of new-type ventricular septal defect occlude in animal model. Acad J Second Milit Med Univ 2004;25:879–81.